Production of $^{154}_{62}$Sm via Intermediate Neutron Capture

William Logan,[1]★
[1]The University of Hull

4 May 2021

ABSTRACT

Heavy elements in stars can be produced in two ways, via the slow and rapid neutron capture processes (*s* and *r* respectively). However, solely using these simulated processes does not accurately depict the heavy element abundance patterns that are observed in carbon enhanced metal poor (CEMP) stars. With the introduction of a new process called the *intermediate* process (*i* process), it is possible to correctly simulate the production of heavy elements that closely match the observed abundance patterns. This paper explores how the abundance of ^{154}Sm changes with the temperature during the *i* process. There is a maximum abundance of 1.08×10^{-9} at a temperature of 1.5×10^{8}K with a peak neutron density of 5.27×10^{11}cm^{3}. The variation of the ^{154}Sm abundance is dependent upon it's production channel via neutron capture onto ^{153}Sm and beta decay of ^{154}Pm. This paper investigates how the temperature can vary the production of these progenitor isotopes and ultimately how that affects the production of ^{154}Sm.

1 INTRODUCTION

Throughout stellar evolution, processes such as the proton-proton chain and the carbon-nitrogen-oxygen (CNO) cycle synthesise most of the lighter elements up until $Z \leq 25$ (iron). Species heavier than iron are increasingly difficult to create, as iron has the lowest binding energy per nucleon, meaning that upon fusion of two iron nuclei, energy is lost. Thus during fusion, all isotopes with a lower mass than iron tend to fuse into it. This is similar to fission, where elements with a higher mass than iron tend to fission into it. Burbidge et al. (1957) proposed two processes that formed elements heavier than iron in neutron rich environments; these are the *s* process and the *r* process. Fig. 1 further reinforces the need to have at least two heavy element nucleosynthesis models due to the two characteristic peaks observed in the region of the higher atomic weights.

1.1 The Classical Processes

1.1.1 The s process

The *s* process is a form of neutron capture, which is the method of species being bombarded with neutrons. Bombarding the species with so many neutrons at one time causes the nucleus to become unstable and eventually decay via the β^- process (Eq. 1), i.e.

$$^{A}_{Z}\mathrm{X} + n \rightarrow {}^{A}_{Z+1}\mathrm{Y} + e^- + \bar{\nu_e}, \tag{1}$$

where X and Y are the isotopes in question, A is the atomic mass, Z is the atomic number, n is a neutron, e^- is an electron and $\bar{\nu_e}$ is an anti neutrino.

For neutron capture to occur, there first must be a source of neutrons. An asymptotic giant branch (AGB) star is typically constituted by 3 distinct regions; the inert carbon and oxygen core, a surrounding helium shell and an outer hydrogen shell. It is theorised that strong convective regions form throughout the star, allowing different isotopes to mix (see Herwig 2005 and references therein). Cameron (1957) was the first to establish that the source of neutrons arose from the mixing of material, resulting in the reaction described in Eq. 2.

$$^{13}_{6}\mathrm{C} + {}^{4}_{2}\mathrm{He} \rightarrow {}^{16}_{8}\mathrm{O} + n \tag{2}$$

Note that there are other methods of producing neutrons but they are not as influential as the ^{13}C$(\alpha, n)^{16}$O. As a result, there is an abundance of free neutrons that can be used in capture (a neutron density of approximately 10^{8}cm^{-3} Lugaro 2005). This is a relatively low neutron density and it limits how heavy an isotope can be produced. To create heavier isotopes, there must be neutron capture onto a species. If the species is unstable, the time between decay must be smaller than that of the time taken to capture for the species to grow heavier. Hence, the *s* process remains close to the valley of stability. The valley of stability is the area in which the stable isotopes of each species reside as shown by the black squares in Fig. 2. At the heavier isotopes, the time taken to decay dominates over the capture time, bringing about a limit at $Z \leq 82$ (lead) (Lugaro 2005). The idea that the maximum neutron density determines the limit of neutron capture remains constant throughout the processes. However, the limit of neutron capture is dependent upon the maximum neutron flux and ultimately, the site at which the process is occurring.

Fig. 2 shows that the *s* process favours the more stable isotopes. There is a build up of isotopes that have the neutron number (N) 82. Rather than the isotopes capturing further onto stable isotopes of the same species, they typically decay back into this chain. This only happens in a couple of places (N=50, 82, 126) and these are known as the magic numbers. The magic numbers are neutron numbers that completely sate the capacity of the neutron shell. For an atom to be completely stable, it must have it's neutron and proton shells filled, similar to electron shells. Thus, there is a build up of isotopes around the neutron magic numbers.

Due to the nature of the *s* process, it requires a relatively mild environment to produce heavier elements, and it does so at a very slow rate. The results of the *s* process are often observed in a companion star as a result of a mass-transfer from the star where the *s* process has taken place (Abate et al. 2016). The outcomes of the *s* process are usually observed in CEMP stars and are very good at showing

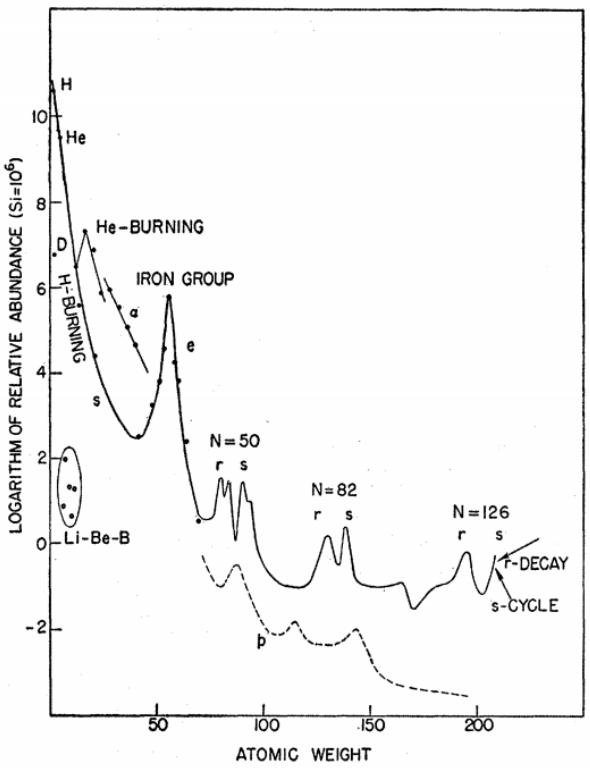

Figure 1. The solar abundance pattern as a function of atomic weight. There is a large peak around the iron atomic weight, where fusion has stopped, resulting in a large abundance of isotopes around iron. There are steeper peaks showing an abundance of isotopes due to the *r* process and broader peaks as a result of the *s* process. Figure taken from Burbidge et al. (1957).

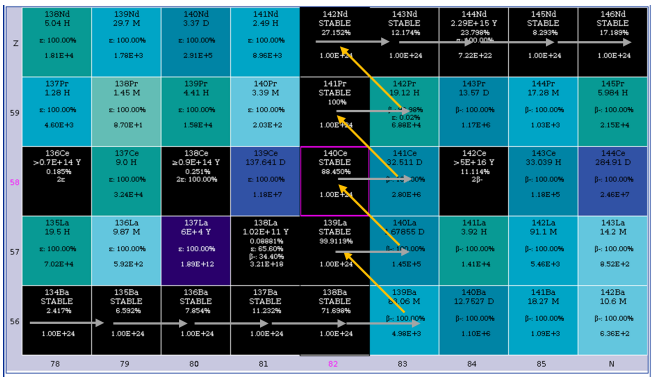

Figure 2. The standard path of the *s* process, where the grey arrows indicate neutron capture and the orange arrows represent beta decay. The black squares are stable isotopes and every other colour is unstable. As soon as there is some abundance of an unstable element, there is little time to capture onto it before it decays, highlighting that the isotopes rarely stray far from stability during the *s* process.

the history of a system due to it's inability to producing anything anomalous.

1.1.2 The r process

Whilst the *s* process occurs in mild conditions, it is thought that the *r* process occurs in extreme conditions, like a neutron star merger

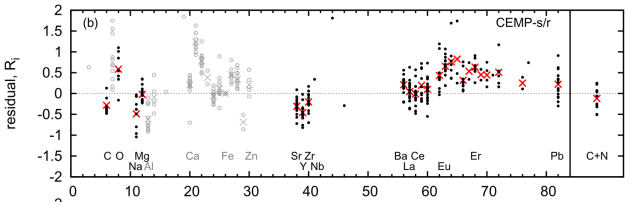

Figure 3. The comparison of the theoretical (through simulation) abundance patterns using the *s*/*r* process to the observed abundance pattern for each molecular weight. If the theorised abundance patterns were to match those of the observed patterns, the plot should be a straight line along the centre of the graph (y=0). Figure taken from Abate et al. (2015).

(Tanvir et al. 2017) or in the less intense site of a core collapse supernova (Thielemann et al. 2011). Due to the nature of the *r* process and where it occurs, a high neutron density is produced (approximately 10^{20}cm^{-3} Lugaro 2005).

As a result of the high neutron flux, the *r* process strays very far away from the valley of stability. With such a large neutron flux, neutron capture on all species occurs within a very small timescale. As there are such small periods of time before each of the captures, there is very little opportunity for each species to decay (Burbidge et al. 1957).

With the neutron density of the *r* process happening in such a short amount of time, very neutron rich materials are created and each species strays very far from the valley of stability. When the neutron flux is reduced, the species can decay and they begin decaying back towards the valley of stability. Naturally, isotopes are produced via the *r* process that are not produced in significant quantities via the *s* process. An example of this would be ^{142}Ce in Fig. 2. To make ^{142}Ce, it would be necessary to neutron capture onto ^{141}Ce, but ^{141}Ce decays before neutron capture can happen, thus rendering ^{142}Ce an *r*-process only material.

1.2 Observational Evidence

CEMP stars are a class of star that show a heavy element abundance pattern and there exists a sub-class called a CEMP-*r*/*s* that can show evidence of the *s* and *r* processes having taken place. When attempting to find the abundance pattern in a star that shows an *s*- and *r*-process signature, there is a large discrepancy between the observed data and the data simulated using the two process. Abate et al. (2015) simulated the abundance produced by both the *s* and the *r* process and compared the outcome to the observed data of a CEMP-*r*/*s* star, finding a noticeable discrepancy (Fig. 3).

One particular way of measuring the balance of *s*-process and *r*-process elements is the barium to europium abundance ratio at any site. Typically, the bigger the build-up of barium, the longer the *s* process has been taking place. 92% of barium is produced via the *s* process Bisterzo et al. (2014), compared to a higher abundance of europium that is observed from the *r* process. However, with the inability for either the *s* or *r* process to occur in CEMP-*r*/*s* stars, there needs to be an explanation as to the origins of the abundances that are seen.

The *i* process is an alternative method to produce heavier species where the *s* process cannot. Cowan & Rose (1977) briefly outlined this method that is in between the *s*/*r* process, that is a plausible method of neutron capture nucleosynthesis. Evidence for the *i* process can be found in CEMP-*r*/*s* stars (Dardelet et al. 2014; Hampel et al. 2019) and this is a very valid starting point to further understand how the process works.

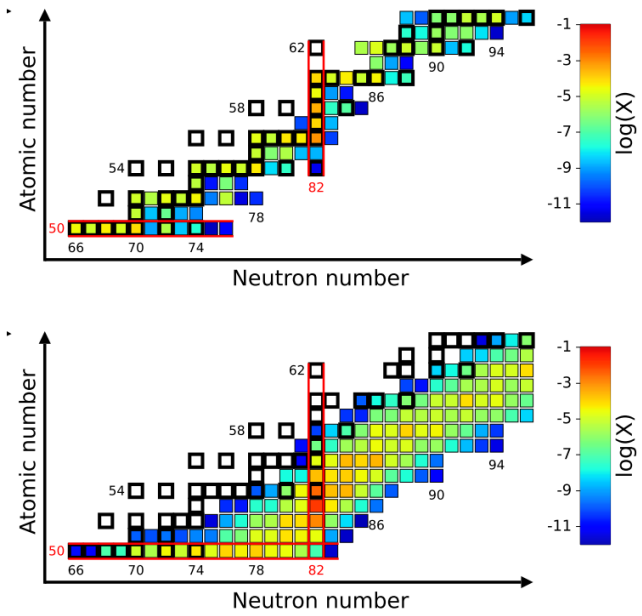

(a) The top panel is the valley of stability during a simulated *s* process, where the black squares represent stable isotopes. During this process, the species rarely stray from the valley of stability. The bottom panel is the valley of stability during a simulated *i* process where the black squares represent the stable isotopes. In this process, the species are typically neutron-rich and a few of the *s*-process isotopes are blocked by *r*-process isotopes, as seen around neutron number 90.

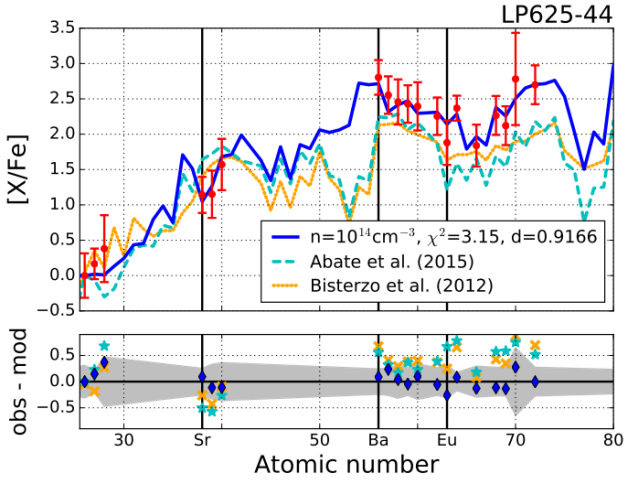

(b) The top panel is the isotope abundance relative to the iron abundance as a function of atomic number. The orange and cyan dashed lines model the *s* and the *r* process and compare that to the observed abundance that is plotted as red points. The dark blue line is the simulation performed by Hampel et al. (2016) using the *i* process. The bottom panel shows the difference in values between the simulated data and the observed data in the star.

Figure 4. Both figures taken from Hampel et al. (2016).

1.2.1 The intermediate neutron capture process

The need for the *i* process is accentuated by Fig. 4b as it is clear that the previously modeled data by Abate et al. (2015); Bisterzo et al. (2012) does not lie within appropriate reason. Hampel et al. (2016) investigated this and established that the *i* process must be occurring in the simulated star, with the simulated data matching closely to the observed data.

In AGB stars where the neutron capture is happening, the shell alternates in burning, known as thermal pulsing. During the thermal pulsing, convective regions form in the outermost hydrogen layer and pull down free neutrons through the entirety of the star (Hampel et al. 2019). In addition there is a large number of ^{13}C isotopes being created and eventually these are used in Eq. 2 to produce a source of free neutrons (Lugaro 2005). This gives rise to approximately 10^{15} cm^{-3} neutrons (Cristallo et al. 2009), and thus giving a short period where there are sufficient neutrons for the *i* process to actually occur. The *i* process is also a neutron capture process and produces more neutron rich and unstable species than the *s* process in a shorter timescale. However, the process tends towards acting similarly to the *r* process where all isotopes are neutron rich. It is aptly named the *intermediate* process as the species stray from the valley of stability but not so far as they do in the *r* process, which can be seen in Fig.4a.

In this paper, I investigate the production of ^{154}Sm via the *i* process and how the temperature affects this supposed *r*-only nuclei.

2 METHOD

To simulate the nucleosynthesis that occurs inside an AGB star, this paper makes use of a one-zone nucleosynthesis code developed by the NuGrid team (Pignatari et al. 2016). It simplifies the conditions of a full simulation to just a few input factors like temperature, density and mass fraction. A one-zone code works by only considering a small amount of material in a space with no outside factors affecting it, with no inflow or outflow of material. Using one-zone code allows for quick runtimes of simulations while also providing very detailed models of the environment of a star.

To understand where the *i* process occurs, the environment that is being simulated must first be defined; temperature, density, initial abundance distribution and network size. The necessary conditions for the site of the *i* process are typically found during proton ingestion episodes, where the star mixes material through its intershell and are typically found in AGB stars (Abate et al. 2016), but the results are observed in CEMP-*r/s* stars.

The size of the network explains which isotopes are used. I used a network of 5627 different isotopes that vary in abundance according to Eq. 3.

$$\frac{dX_i}{dt} = R_i - S_i, \tag{3}$$

where X_i is the mass fraction of the i_{th} species in the network and R_i, S_i are the reactions producing and destroying species i, respectively.

For the composition, I used an intershell region of a star, with a constant mass of 1.65M$_\odot$ and a metallicity of $Z = 10^{-3}$. Finally, I used a constant density of $1\times10^3 gcm^{-3}$ and I varied the temperature between runs (keeping the temperature constant throughout each of the simulations run). I chose to vary the temperature between simulations to imitate two things, the site at which the *i* process is occurring and to consider the different depths at which the process can happen in a star (Herwig et al. 2008; Stancliffe & Lattanzio 2011).

To determine the dependence of ^{154}Sm on temperature, I compared the abundance of ^{154}Sm produced to the different temperatures at the production sites. Similar to ^{142}Ce in Fig. 2, ^{154}Sm is considered an *r*-only isotope. The theory of the *s*/*r* processes can be applied to discover the production pathways of ^{154}Sm at different temperatures.

3 RESULTS

The production of ^{154}Sm is heavily dependent upon the neutron flux as it is not produced from any stable isotopes since to produce heavier isotopes, the capture rate must be higher than that of the decay rate. The two ways of producing ^{154}Sm are either from neutron capture onto ^{153}Sm or from beta decay from ^{154}Pm. Both of these isotopes are unstable and to produce these exact isotopes in abundance is not common. Thus, for a significant abundance of ^{154}Sm to be produced, there must first be a significant amount of ^{154}Pm or ^{153}Sm.

To determine the impact of temperature on the production of ^{154}Sm, an initial simulation was performed with a temperature of 1×10^8K resulting in a peak abundance of 5.86×10^{-10} of ^{154}Sm (Fig. 5a). This is where is the lowest peak neutron densities are seen and at this temperature there is a constant neutron density of 4.23×10^7cm^3 for 10^8 seconds. However, Fig. 5b indicates the full production pathway of ^{154}Sm at this temperature. In this case, there is very little to no production of ^{154}Pm and therefore the only way that ^{154}Sm can be produced is via neutron capture onto ^{153}Sm. Fig. 5b does not show any arrow from ^{153}Sm to ^{154}Sm because only a few reactions are happening. Since there is no ^{154}Pm produced, the only viable production is via neutron capture onto ^{153}Sm.

At a temperature of 2×10^8K, there is also an increase in peak neutron density of 8.57×10^{13}cm^3 for 10^3 seconds and an increased peak abundance of ^{154}Sm at a value of 3.14×10^{-8} (Fig. 5c). At this temperature, there is a higher peak neutron flux compared to a temperature of 1×10^8K. This results in an abundance of 4.61×10^{-9} of the unstable isotope ^{154}Pm, a progenitor isotope to ^{154}Sm like ^{153}Sm. For further clarification, Fig. 5d shows that the main production of ^{154}Sm arises from the neutron capture from ^{153}Sm, with some beta decay of ^{154}Pm. However, the chart reveals that the majority of ^{154}Pm is capturing neutrons rather than decaying into ^{154}Sm. In this model, the production of ^{154}Sm is via neutron capture onto ^{153}Sm similar to the mechanism at a temperature of 1×10^8K.

Increasing the temperature to 3×10^8K results in a peak neutron density of 6.96×10^{14}cm^{-3} at a time of 10^3 seconds and a later peak of 1.69×10^{11}cm^{-3} at a time of 10^6 seconds (Fig. 5e). At the first peak, there is a similar abundance of all isotopes with similar weight. Fig. 5f depicts an equal production of ^{154}Sm via neutron capture of ^{153}Sm and decay of ^{154}Pm. Fig. 5f alludes to the fact that at this temperature, the simulation acts similarly to the *r* process, by producing neutron-rich isotopes in a short timescale. However, at the second peak, there is an abundance of 1.77×10^-10 ^{153}Sm and an abundance of 1.13×10^{17} ^{154}Pm at a time of 10^6 seconds. There is a much larger amount of ^{153}Sm than ^{154}Pm and therefore it is more likely that the production of ^{154}Sm arises from the neutron capture onto ^{153}Sm. This can be reinforced by comparing the neutron density peak around this time to the neutron density of an earlier simulation, where the main production method of ^{154}Sm is via the neutron capture onto ^{153}Sm.

Considering the range of temperatures through the simulations that were run, there is a link that can be established between neutron flux and ^{154}Sm abundance. To produce significant amounts of ^{154}Sm requires a sufficient timescale with a viable neutron flux. These models suggest a suitable set of conditions where the *i* process can occur and hopefully in the future, it can be observed by using the abundance of some *r*-only nuclei (e.g. ^{154}Sm and ^{142}Ce).

Table 1 concludes the outcomes from all of the simulations that have been run. It indicates that the highest abundance of ^{154}Sm occurs at a high peak neutron density at a relatively low temperature of 1.5×10^8K.

Temperature ($\times 10^8$K)	Time (s^{-1})	Peak Neutron Density (cm^3)	Peak ^{154}Sm Abundance Mass fraction
1.0	4.23×10^7	10^4	5.86×10^{-10}
1.5	5.27×10^{11}	10^4	1.02×10^{-7}
2.0	8.57×10^{13}	$10^{3.5}$	3.14×10^{-8}
2.5	6.61×10^{14}	$10^{3.5}$	4.92×10^{-8}
3.0	6.96×10^{14}	10^3	1.08×10^{-9}

Table 1. The table highlights the increase of peak neutron densities with increasing temperatures.

4 DISCUSSION

While the work done in this paper provides a detailed analysis of the production of an *r*-only nuclei, there remains some limitations to the simulation. For example, in this paper I have used a one-zone code which does not consider mixing of material. If I had used a multi-zone code, which considers the star as a whole and not a small container like one-zone code, I may have obtained different results due to the interaction between matter.

Moreover, this paper has assumed that all conditions remain constant over the large timescale chosen. Keeping these conditions constant does not account for the evolution of the star and how the environment changes with time. It may be that the production of Eq. 2 decreases with time and therefore the production of heavier isotopes also decreases. Variable conditions can also account for multiple thermal pulses and proton ingestion episodes, though this is something that can be explored in detail in a later study.

Regardless of consideration of limitations, there will always be uncertainty in produced results. This is associated mainly with the nuclear reaction rates, which include the chance to neutron capture and the chance to beta decay. There is the potential that the reaction rates of specific species increases or decreases with temperature and thus alter acquired outcomes.

Work done by Travaglio et al. (2001) on galactic evolution yields a heavy isotope distribution similar to that produced in this work. Where I have focused on the particular production of an unexpected isotope ^{154}Sm, Travaglio et al. (2001) has focused on the overall abundance of all isotopes without referencing any detail about their production pathways. There are more *r*-only nuclei that can be observed in CEMP-*r/s* stars and we leave this to further study to confirm if their production mechanisms are similar to the findings in this paper.

The original definition of the *i* process defined by Burbidge et al. (1957) was used in this paper and has been shown to follow their outlined predictions. Burbidge et al. (1957) speculated the idea of a process in between the *s* process and the *r* process as there is a large difference between the two neutron densities (10^8cm^{-3} and 10^{20}cm^{-3} respectively, Lugaro 2005). In this paper I have simulated a range of temperatures and proposed that the *i* process is occurring between a temperature of 1.5×10^8K and 2.5×10^8K, producing a neutron flux between 10^{11}cm^{-3} and 10^{14}cm^{-3}. This further reinforces the need and the existence of a third, intermediary process that was predicted by Burbidge et al. (1957).

Finally, Hampel et al. (2019) has simulated the *i* process, confirming its importance alongside the two classical processes. This paper has taken the work of Hampel et al. (2019) one step further, looking specifically at how the *i* process can explain some of the heavy element abundance patterns that cannot be explained using the two classical processes.

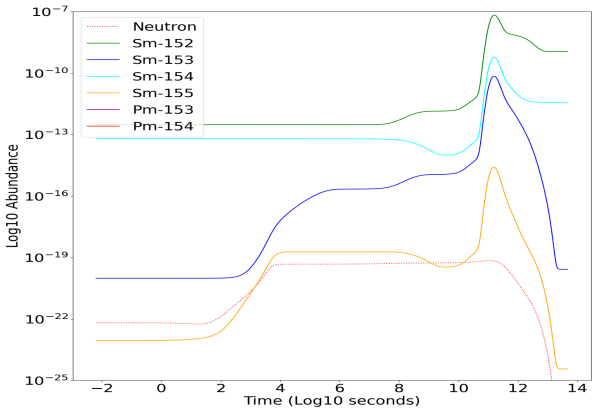

(a) A plot of mass fraction abundance as a function of the time. A peak abundance of 3.53×10^{17}cm^3 of ^{154}Sm occurs at a time of approximately 10^{12} seconds and the peak neutron abundance of 4.23×10^7cm^3 at a time of 10^4 seconds, remaining constant for 10^8 seconds.

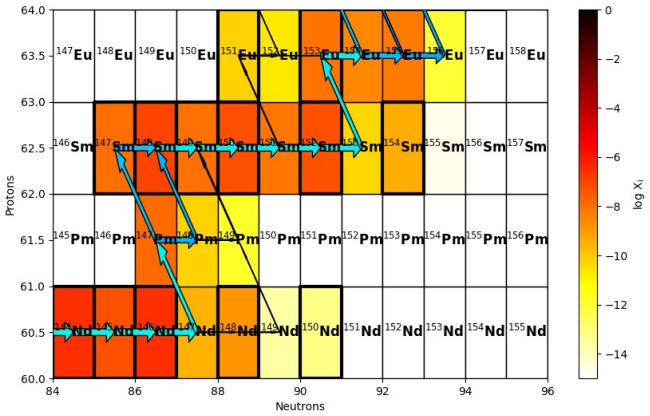

(b) A chart showing the abundance and production of the isotopes around ^{154}Sm at the peak neutron density. The black outlined squares show the stable elements, the colours represent how abundant each isotope is and the size of the arrows show how many reactions between the respective isotopes are occurring. The distribution of isotopes remains close to the valley of stability with large amounts of stable isotopes.

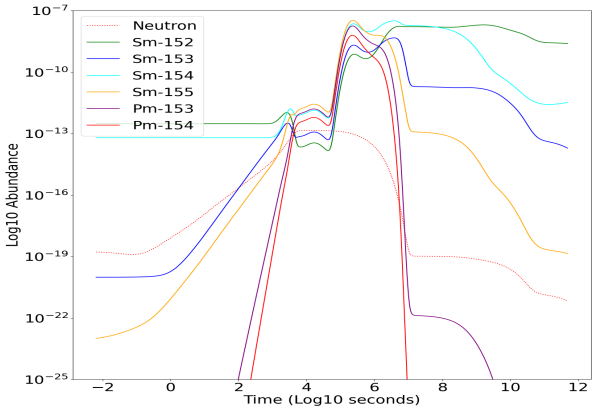

(c) A plot of mass fraction abundance as a function of the time. A peak abundance of 1.89×10^{19}cm^3 of ^{154}Sm occurs at a time of 10^5 seconds and the peak neutron abundance of 8.57×10^{13}cm^3 at a time of approximately $10^{3.5}$ seconds remaining constant for 10^2 seconds.

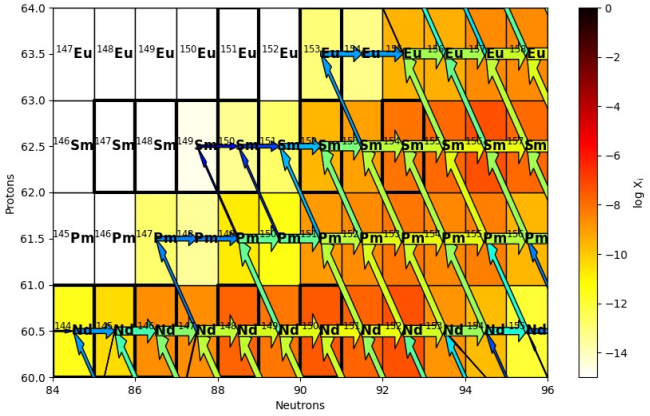

(d) A chart showing the abundance and production of the isotopes around ^{154}Sm at the peak neutron density. The black outlined squares show the stable elements, the colours represent how abundant each isotope is and the size of the arrows show how many reactions between the respective isotopes are occurring. The chart shows the species straying from the valley of stability, producing unstable and neutron rich isotopes.

Figure 5. Panels a) and b) show details of the T=1×10^8 K run. Panels c) and d) are for the T=2×10^8 K run.

5 CONCLUSION

To conclude, this paper has probed the method of production of ^{154}Sm via the intermediate neutron capture process. It can be seen that there is a clear variation of abundance, with a small change in temperature, by orders of magnitude. Ideally, this investigation can be applied to look at other *r*-only nuclei to show that they can be produced via the *i* process without requiring such extreme conditions as the *r* process demands.

To further investigate the production of ^{154}Sm via the *i* process, more simulations would need to be produced with a larger variation of temperatures. Another aspect to explore would be the initial conditions such as density or mass fraction of the star, as this impacts the production of heavy elements as well as the temperature (Stancliffe & Lattanzio 2011). It would also be beneficial to run the simulation on a bigger scale that can incorporate hydrodynamics and stellar evolution code to closely simulate the processes occurring in the stars that we observe.

REFERENCES

Abate C., Pols O. R., Izzard R. G., Karakas A. I., 2015, A&A, 581, A22
Abate C., Stancliffe R. J., Liu Z.-W., 2016, A&A, 587, A50
Bisterzo S., Gallino R., Straniero O., Cristallo S., Käppeler F., 2012, Monthly Notices of the Royal Astronomical Society, 422, 849
Bisterzo S., Travaglio C., Gallino R., Wiescher M., Käppeler F., 2014, The Astrophysical Journal, 787

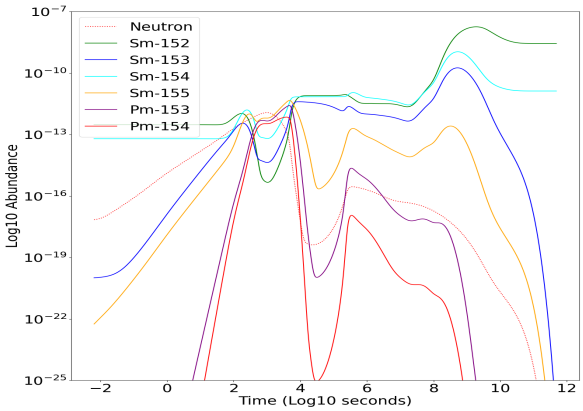

(e) A plot of mass fraction abundance as a function of time. The plot does not show a sustained amount of time where the neutron density remains constant, but there is a peak of 6.52×10^{17}cm^3 of ^{154}Sm at a time of 10^3 seconds and a peak neutron density of 6.96×10^{14}cm^3.

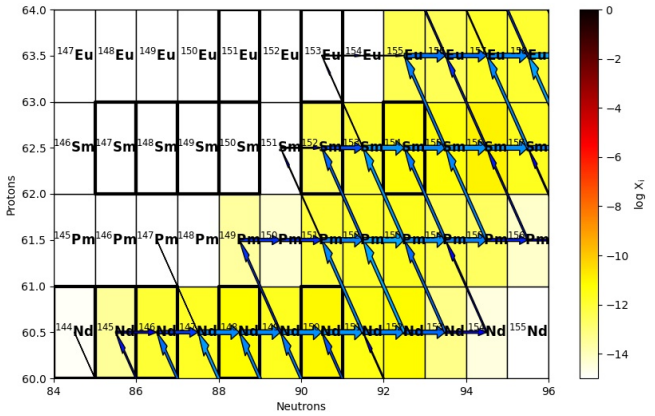

(f) A chart showing the abundance and production of the isotopes around ^{154}Sm at the peak neutron density. The black outlined squares show the stable elements, the colours represent how abundant each isotope is and the size of the arrows show how many reactions between the respective isotopes are occurring. The chart shows a similar abundance of each isotope around ^{154}Sm with an arrow coming from both ^{153}Sm and ^{154}Pm.

Figure 5. Panels e) and f) show details of the T=3×10^8 K run.

Burbidge E. M., Burbidge G. R., Fowler W. A., Hoyle F., 1957, Rev. Mod. Phys., 29, 547
Cameron A. G. W., 1957, The Astronomical Journal, 62, 138
Cowan J. J., Rose W. K., 1977, The Astrophysical Journal, 212, 149
Cristallo S., Piersanti L., Straniero O., Gallino R., Domínguez I., Käppeler F., 2009, Publications of the Astronomical Society of Australia, 26, 139
Dardelet L., et al., 2014, Proceedings of Science, 07-11-July-2015, 7
Hampel M., Stancliffe R. J., Lugaro M., Meyer B. S., 2016, The Astrophysical Journal, 831, 171
Hampel M., Karakas A. I., Stancliffe R. J., Meyer B. S., Lugaro M., 2019, ApJ, 887, 11
Herwig F., 2005, Annual Review of Astronomy and Astrophysics, 43, 435
Herwig F., et al., 2008, in Nuclei in the Cosmos (NIC X). p. E23 (arXiv:0811.4653)
Lugaro M., 2005, Stardust from Meteorites. World Scientific Series in Astronomy and Astrophysics Vol. 9, WORLD SCIENTIFIC, doi:10.1142/5705
Pignatari M., et al., 2016, The Astrophysical Journal Supplement Series, 225, 24
Stancliffe R. J., Lattanzio J. C., 2011, 445, 29
Tanvir N. R., et al., 2017, The Astrophysical Journal, 848, L27
Thielemann F. K., et al., 2011, Progress in Particle and Nuclear Physics, 66, 346
Travaglio C., Gallino R., Busso M., Dalmazzo A., 2001, Mem. Soc. Astron. Italiana, 72, 381

This paper has been typeset from a TEX/LATEX file prepared by the author.